JACS
JOURNAL OF THE AMERICAN CHEMICAL SOCIETY

Article

pubs.acs.org/JACS

Electrochemical Shell-Isolated Nanoparticle-Enhanced Raman Spectroscopy: Correlating Structural Information and Adsorption Processes of Pyridine at the Au(hkl) Single Crystal/Solution Interface

Jian-Feng Li,*[,†,‡] Yue-Jiao Zhang,[†] Alexander V. Rudnev,[‡] Jason R. Anema,[†] Song-Bo Li,[†] Wen-Jing Hong,[‡] Panneerselvam Rajapandiyan,[†] Jacek Lipkowski,[§] Thomas Wandlowski,[‡] and Zhong-Qun Tian[†]

[†]MOE Key Laboratory of Spectrochemical Analysis and Instrumentation, State Key Laboratory of Physical Chemistry of Solid Surfaces, College of Chemistry and Chemical Engineering, Xiamen University, Xiamen 3605, China

[‡]Department of Chemistry and Biochemistry, University of Bern, Freiestrasse 3, Bern CH-3012, Switzerland

[§]Guelph-Waterloo Center for Graduate Work in Chemistry, Department of Chemistry and Biochemistry, University of Guelph, Guelph, Ontario N1G 2W1, Canada

Supporting Information

ABSTRACT: Electrochemical methods are combined with shell-isolated nanoparticle-enhanced Raman spectroscopy (EC-SHINERS) for a comprehensive study of pyridine adsorption on Au(111), Au(100) and Au(110) single crystal electrode surfaces. The effects of crystallographic orientation, pyridine concentration, and applied potential are elucidated, and the formation of a second pyridine adlayer on Au(111) is observed spectroscopically for the first time. Electrochemical and SHINERS results correlate extremely well throughout this study, and we demonstrate the potential of EC-SHINERS for thorough characterization of processes occurring on single crystal surfaces. Our method is expected to open up many new possibilities in surface science, electrochemistry and catalysis. Analytical figures of merit are discussed.

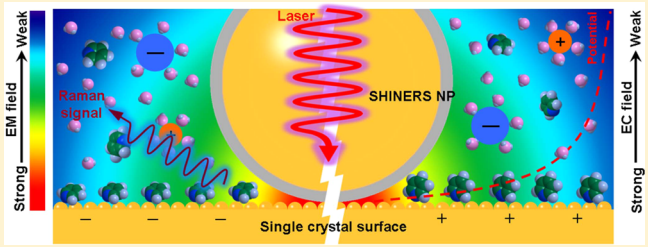

INTRODUCTION

Pyridine has become a standard probe molecule in studies of coordination and the resulting orientation of molecules at interfacial metal surfaces.[1−3] Pyridine adsorption has been examined by electrochemical techniques,[4,5] electroreflectance (ER) spectroscopy,[6] second harmonic generation (SHG),[7] difference frequency generation (DFG),[8] scanning tunneling microscopy (STM),[9,10] and surface-enhanced infrared absorption (SEIRA).[10] These investigations have shown that pyridine can bind to Au low index facets in both π-bonded (flat) and σ-bonded (vertical/tilted) orientations through its aromatic ring and its nitrogen atom, respectively. They have also shown that the adsorption process is strongly dependent on the electrode's charge and the crystal structure of its surface. The methods used in these studies have provided a fair understanding of pyridine adsorption, but the structural information that each can offer has its limitations. Few comprehensive reports on the correlation of their results have been published.

Surface-enhanced Raman spectroscopy (SERS)[11−13] is a nondestructive and ultrasensitive vibrational spectroscopy that provides rich structural information.[14−19] It has been used to characterize adsorption on metal electrode surfaces, and to elucidate reaction mechanisms at electrochemical, biological, and other important interfaces.[2,20−26] Pyridine has a large Raman scattering cross-section, and for a variety of reasons that involve both its properties and its history, it has become one of the most extensively used model analytes in SERS investigations.[11−13,24] Many SERS-based studies of pyridine in different electrochemical systems have been published over the past few decades, covering experimental and theoretical aspects.[24,27−31] However, SERS is limited by a lack of substrate generality.[32] It is not suitable for the examination of smooth surfaces, which do not support surface plasmon resonance (SPR).[33−38] Therefore, most of these studies have been restricted to roughened surfaces that are not well-defined. Spectral interpretation may be complex, and SERS from atomically smooth single crystals would be a great asset to study adsorption phenomena unambiguously. Raman studies of single crystal surfaces have proven extremely difficult, and few have been carried out on true atomically flat surfaces,[39] e.g., by using attenuated total reflection (ATR)[40] and tip-enhanced Raman spectroscopy (TERS).[41−43] Neither of these methods is appropriate for use in a wide range of applications, and major challenges remain.

Received: December 30, 2014
Published: January 27, 2015

DOI: 10.1021/ja513263j
J. Am. Chem. Soc. 2015, 137, 2400−2408

Recently, our group developed a new approach called "shell-isolated nanoparticle-enhanced Raman spectroscopy" or "SHINERS"[44] to solve this problem. Here, gold-core silica-shell ($Au@SiO_2$) nanoparticles are used to enhance Raman signals from species on atomically flat single crystal surfaces. The Au cores act to support SPR modes and boost electromagnetic field strength in localized regions at the single crystal/solution interface. The ultrathin yet pinhole-free silica shells act to separate the Au cores from the system under study and ensure that there is no interference from processes involving the Au cores. This method has already been applied to a number of challenging systems.[44−53] For example, enhancement factors obtained for pyridine on single crystal Au and Pt surfaces using SHINERS nanoparticles are comparable to those obtained using bare Au nanoparticles because hotspots are transferred to nanoparticle-surface gaps from nanoparticle−nanoparticle gaps.[49]

In the present work, we combine electrochemical methods with SHINERS (EC-SHINERS) for the in situ monitoring of pyridine adsorption on Au(hkl) single crystal electrode surfaces. The effects of crystallographic orientation, pyridine concentration and applied potential are all examined in detail. Our electrochemical and spectroscopic results correlate very well, and remarkably, EC-SHINERS revealed for the first time the formation of a second pyridine adlayer on Au(111). By fully characterizing pyridine adsorption on Au low index facets, we demonstrate the great potential of EC-SHINERS in electrochemistry and surface science.

A schematic diagram of our method appears in Figure 1. It is sensitive enough to examine a monolayer, selective for an adsorbate on the surface of an electrode, and uniquely suited to provide a wealth of information about processes occurring in the double layer region. We anticipate that it may also be used to monitor reaction pathways, understand the correlations that exist between structure and reactivity for a wide range of interfacial phenomena, and even provide new opportunities for experimental study of the SERS selection rule.

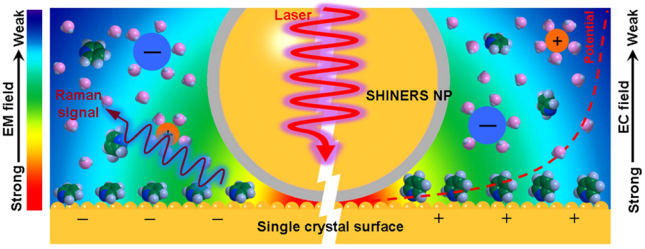

Figure 1. A schematic diagram of EC-SHINERS. The coexistence of electromagnetic (EM) and electrochemical (EC) fields is shown, with the electrode surface more negative at the left and more positive at the right.

RESULTS AND DISCUSSION

Preparation of SHINERS Nanoparticles and Their Addition to Au(hkl) Single Crystal Electrodes. 55 nm Au nanoparticles were prepared according to Frens' method[54] for use as the SHINERS nanoparticle core. First, 200 mL of 0.29 mM chloroauric acid were brought to a boil with stirring. Then, to obtain Au nanoparticles with a 55 nm diameter, 1.4 mL of 39 mM trisodium citrate were added quickly to the boiling solution (nanoparticle diameter can be adjusted by varying the amount of trisodium citrate solution added[54]). The resulting mixture was refluxed with stirring for 40 min and allowed to cool to room temperature.

Next, an ultrathin yet pinhole-free silica shell was added to the Au core. This was accomplished by placing 30 mL of the Au nanoparticle solution (0.29 mM) and 0.4 mL of 1 mM (3-aminopropyl)trimethoxysilane in a round-bottom flask and stirring for 15 min at room temperature. Separately, a 27% solution of sodium silicate (from Sigma-Aldrich) was diluted to 0.54% (90.0 mM) and adjusted to a pH of about 10.3 using hydrochloric acid. 3.2 mL of the diluted and acidified sodium silicate solution were then added to the reaction mixture and it was stirred for 3 more min at room temperature. The round-bottom flask was placed in a 90 °C water bath and stirred for a period of time. The shell thickness can be tuned from a few nanometers to tens of nanometers simply by controlling the reaction time. For example, 20 min of heating will give a shell thickness of about 2 nm and 1 h of heating will give a shell thickness of about 4 nm.[44,55,56] In the present work, we stirred for 30 min to obtain a 2 to 3 nm silica shell (Figure 2A).

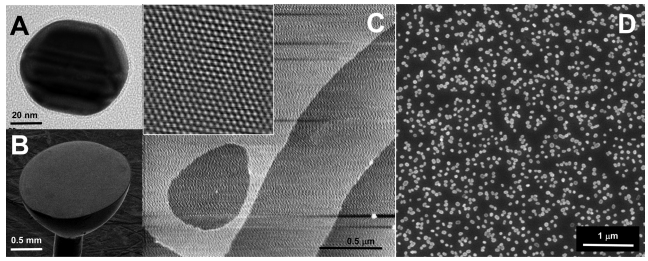

Figure 2. (A) High-resolution TEM image of a 55 nm Au NP with a 2 nm SiO_2 shell. (B) SEM image of a Au(111) half-bead single crystal electrode. (C) AFM and high-resolution (5.3 nm × 5.3 nm) STM images of an island-free Au(111)-(1 × 1) surface. (D) SEM image of SHINERS nanoparticles on a Au(111) single crystal electrode.

Electromagnetic field strength decreases exponentially with distance from the enhancing surface,[57] which is the surface of the Au core in this case, but a 2 to 3 nm shell provides sufficient enhancement of pyridine Raman signals. It is also thick enough to ensure a lack of pinholes.

The hot mixture was then transferred into some 1.5 mL test tubes and cooled in an ice bath to stop the reaction. These test tubes were centrifuged at 5500 rpm for 15 min and the supernatant was removed. The concentrated solution of SHINERS nanoparticles at the bottom of each test tube was diluted with Milli-Q water, the SHINERS nanoparticles were centrifuged again, and the supernatant was removed a second time. After rinsing in this way, the clean and concentrated $Au@SiO_2$ nanoparticle solution occupied a volume of about 200 μL and had a nanoparticle concentration of about 2.0 mM. Both the electrochemical and SERS tests for a lack of pinholes in the shell, which have been described in previous publications,[44,55,56] were performed.

Two microliters of this solution were dropped onto a freshly prepared Au(hkl) single crystal bead electrode using a pipet, and dried under a vacuum (the Au(111) electrode is shown in Figure 2B,C). The nanoparticle coverage (Figure 2D) was estimated to be about 20 to 40% by calculating the number of nanoparticles in the sol and confirming by scanning electron microscopy (SEM).[58]

Modifying an electrode with SHINERS nanoparticle solution may lead to contamination of its surface. For this reason, $Au@SiO_2$ nanoparticle modified electrodes were cleaned using the

DOI: 10.1021/ja513263j
J. Am. Chem. Soc. 2015, 137, 2400−2408

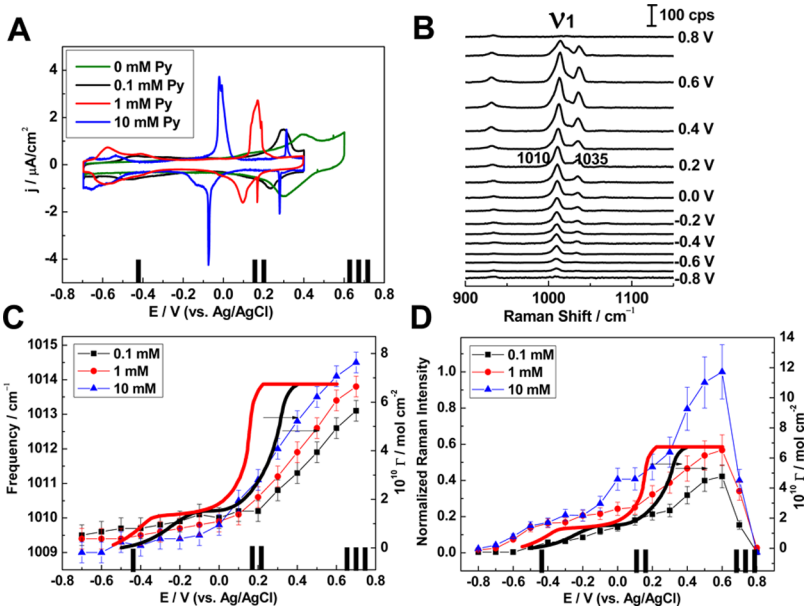

Figure 3. (A) CVs from a Au(111) electrode in 0.1 M $NaClO_4$ solution without pyridine (Py) and with Py at 0.1, 1, and 10 mM. (B) SHINER spectra of Py adsorption on a Au(111) electrode in 0.1 M $NaClO_4$ + 1 mM Py. Acquisition time was 30 s. The dependence of Raman frequency (C) and normalized Raman intensity (D) on applied potential for the Py ν_1 ring breathing mode (data points connected by straight lines), and these are compared to surface concentration isotherms[59] (bold curves).

hydrogen evolution reaction (HER) as described in a previous publication.[58] The electrode was thoroughly rinsed with Milli-Q water and transferred to a homemade electrochemical cell containing 0.1 M $NaClO_4$. The cell was oriented vertically, and the working electrode was positioned near the quartz optical window to establish a thin electrolyte film (<50 μm) between them. A potential of −2.0 V was applied and the HER proceeded vigorously, but the geometry of the cell and its components prevented the formation of large hydrogen bubbles and kept the submonolayer of nanoparticles rather stable. Under such conditions, impurities desorb from the surface and move into solution. After roughly 1 min, the electrolyte solution was replaced. This HER cleaning procedure was repeated 3 or 4 times. The electrode was then removed from the electrochemical cell and rinsed with Milli-Q water. It was immersed in 10 mM hydrochloric acid for 10 min to lift the reconstruction, which can partially recover during HER treatment. After rinsing the electrode again with Milli-Q water and drying in a stream of argon, it was placed in an electrochemical cell or spectroelectrochemical cell for the desired experiment. HER cleaning was proven effective and nondestructive for single crystal surfaces by both cyclic voltammetry (Supporting Information Figures S1, S2 and S3) and Raman spectroscopy.[58]

Pyridine Adsorption on Au(111). Typical cyclic voltammograms (CVs) from a Au(111) electrode in 0.1 M $NaClO_4$ solution, with pyridine absent or present in various concentrations (0.1, 1, and 10 mM), are given in Figure 3A. They were recorded at a rate of 10 mV/s in the potential range −0.7 to 0.6 V (versus Ag/AgCl). Hydrogen evolution occurs at potentials more negative than −0.7 V, and Au is oxidized at potentials more positive than 0.6 V. Here and further, we divide the potential dependence of current and spectral characteristics into three regions: (I) adsorption of pyridine at negative potentials, (II) a pyridine adlayer phase transition coupled with lifting of the surface reconstruction, and (III) Au surface oxidation leading to pyridine desorption at positive potentials. Their potential windows depend on crystallographic face and pyridine concentration. CVs obtained in the presence of pyridine were not extended into region III so that Au surface oxidation/reduction would not affect the pyridine signals in the reverse scan.

The positive scan obtained for the pyridine-free solution displays a broad peak at 0.4 V, which has been assigned to adsorption of the electrolyte anion and lifting of the $(p \times \sqrt{3})$ reconstruction.[59] Anion desorption and partial recovery of the $(p \times \sqrt{3})$ reconstruction takes place in the negative sweep, and results in the counter peak at 0.3 V.

For the solutions containing pyridine at $E < -0.2$ V (region I), broad signals in the positive and negative scans have been assigned to pyridine adsorption and desorption, respectively.[59]

The most pronounced features are the anodic peaks at 0.30, 0.15, and −0.01 V for 0.1, 1, and 10 mM pyridine respectively (region II). Both the anodic and cathodic peaks shift to more negative potentials with increasing pyridine concentration. Stolberg et al.[59] have proposed, based on chronocoulometric and differential capacitance data, that pyridine adsorbs on Au(111) in two different configurations: an aromatic ring π-bonded flat orientation at negative potentials and a nitrogen atom σ-bonded vertical/tilted orientation at positive potentials. They found that the transition occurs at 0.30 V for 0.1 mM pyridine and at 0.15 V for 1 mM pyridine. These potentials are consistent with the positions of the anodic peaks in the CVs presented here. The cathodic peaks are due to the reverse process, a reorientation of pyridine from vertical/tilted to flat.

The 1 and 10 mM pyridine CVs also display sharp current spikes that overlap with the most pronounced peaks in both the positive and negative scans. These spikes may correspond to the formation of ordered domains of N-bonded pyridine on (111) terraces. In situ STM[9,10] has revealed an ordered structure of N-bonded pyridine on Au(111) film electrodes at potentials near the main peaks. We note that these narrow spikes were not observed in CVs from defect rich Au(111) film

DOI: 10.1021/ja513263j
J. Am. Chem. Soc. 2015, 137, 2400−2408

electrode surfaces and appear to be characteristic of well-ordered single crystal electrodes.

Finally, Au surface oxidation leads to the desorption of pyridine (region III).

Figure 3B shows in situ SHINER spectra of pyridine adsorption on a Au(111) single crystal electrode from 1 mM solution. The electrode potential was increased from −0.8 to 0.8 V in 0.1 V increments, with about 2 min at each step for stabilization of the current and subsequent acquisition of the spectrum. The 550 to 1700 cm^{-1} spectral range contains all of the most significant peaks (Supporting Information Figure S4). The grating was not changed during acquisition of the spectra so that even slight differences in the frequency of the peaks could be compared. The strong peaks at 1010 and 1035 cm^{-1} are due to the ν1 ring breathing mode and the ν12 symmetric triangular ring deformation mode of pyridine respectively (Figure 3B).[29,60] The other weak bands at around 630, 1210, and 1600 cm^{-1} (Supporting Information Figure S4) have been assigned to the ν6a, ν9a and ν8a modes, respectively.[29,60]

Potential dependent spectral features yield key information about the three regions. The ν1 mode frequency is plotted against potential in Figure 3C (data points connected by straight lines). In region I, it is fairly constant. In region II, however, the frequency increases continuously with the electrode potential (beginning at 0.2, 0.1, and 0.0 V for the 0.1, 1, and 10 mM pyridine concentrations) with a Stark tuning rate of about 5.6 cm^{-1}/V. This marks a change in the orientation of pyridine. The frequency of the ν1 ring breathing mode is lower for the flat orientation due to the weak binding interaction between π-orbitals and the metal, while it is higher for the vertical orientation because of the strong interaction between nitrogen atom lone-pair electrons and the metal.[24,61] Figure 3C therefore indicates that pyridine is flat adsorbed in region I and vertically adsorbed in region II. This result supports the proposal, based on an extensive analysis of chronocoulometric data made previously by Stolberg et al.,[59] that the coverage potential dependences (bold curves in Figure 3C) demonstrate pyridine forms a full monolayer on Au(111) in region II.

At E > about 0 V in region II, ν1 frequency is higher for greater pyridine solution concentrations (i.e., blue data points > red data points > black data points at a given potential). This means that on formation of a full monolayer at a positive potential, the binding interaction between pyridine and Au(111) becomes stronger with increasing pyridine solution concentration. This is probably because the potential of zero charge (E_{pzc}) shifts negatively with increasing pyridine solution concentration, which is reflected by the negative shift in region II CV peak position (Figure 3A). Thus, at a given potential, the electrode surface is charged more positively in 10 mM pyridine than it is in 0.1 mM pyridine and this leads to a stronger binding interaction between the molecule and the Au(111) surface.

The ν1 mode intensity is plotted against potential in Figure 3D (data points connected by straight lines). As the potential is stepped in the positive direction, ν1 intensity reaches a maximum at 0.6 V and then drops to zero at 0.8 V. Changes in the local optical field due to the dipole−dipole depolarization mechanism contribute to the intensity maximum in the plateau of the adsorption isotherm.[27] In the SHINER spectra (Supporting Information Figure S4), a new band appears at about 585 cm^{-1} when the potential reaches 0.7 and 0.8 V. We attribute this new peak to surface oxidation,[62] and we believe that surface oxidation causes pyridine desorption, which is seen as the ν1 intensity drop in region III.

It is known from chronocoulometric, SHG and ER spectroscopy data[59,63] that the coverage of pyridine increases with increasing potential in region I (bold curves in Figure 3D), and that there is an orientation change from flat to vertical in region II where a full monolayer of N-bonded pyridine is adsorbed. The greater pyridine coverage at more positive potentials in region I results in a higher ν1 intensity. As well, the orientation change from flat to vertical yields an increase in ν1 intensity according to the SERS selection rule.[24] Indeed, the intensity increases at 0.3, 0.1, and −0.1 V (Figure 3D) coincide with the phase transition potentials in the CVs (Figure 3A) for 0.1, 1, and 10 mM pyridine.

The ν1 intensity continues to increase as the potential is stepped in region II, where coverage is constant and pyridine is vertically adsorbed rather than flat. The continued increase may indicate that pyridine becomes less tilted and more truly vertical on the Au(111) surface at more positive potentials in region II. A stronger binding interaction between pyridine and Au at more positive potentials has been observed by subtractively normalized interfacial Fourier transform infrared spectroscopy (SNIFTIRS),[64] and this may also cause the ν1 intensity to increase in region II. At more positive potentials, the lone-pair of electrons on the nitrogen atom are more strongly coordinated to the Au surface.[24,29]

A very interesting phenomenon, which has never been reported, occurs for 10 mM pyridine only on a Au(111) surface. One more pair of spikes appear at ∼0.3 V in the CV (Figure 4A), and simultaneously, a new feature appears at 1003 cm^{-1} in the SHINER spectra (Figure 4B). We believe that these changes indicate formation of a second pyridine adlayer.

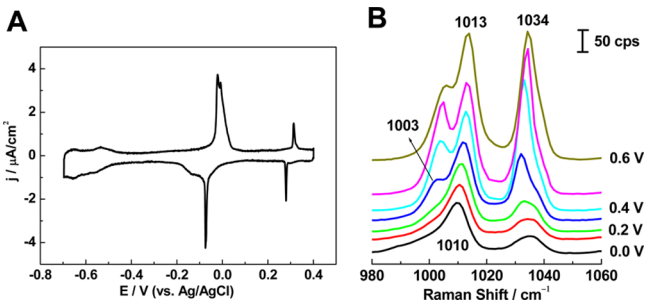

Figure 4. (A) CV from a Au(111) electrode in 10 mM pyridine + 0.1 M $NaClO_4$ solution. (B) SHINER spectra of pyridine adsorbed on the Au(111) electrode between 0.0 and 0.6 V.

First, the frequency of the new SHINERS peak is nearly identical to the ν1 frequency of aqueous pyridine (∼1003 cm^{-1}) and quite different from what is seen for pyridine chemisorbed on Au (∼1012 cm^{-1}).[24] This indicates a weak interaction between pyridine and the Au surface. Second, both the intensity and the frequency of the 1003 cm^{-1} feature increase with applied potential. This would not be the case if the feature originated from bulk pyridine. Third, the current spikes at ∼0.3 in the CV suggest a phase transition within the adsorbed pyridine. Since the frequency of the main ν1 band at ∼1012 cm^{-1} shows no abrupt change between 0.2 and 0.4 V (Figure 3C), the current spikes cannot be assigned to a phase transition within the first pyridine adlayer.

Pyridine multilayer formation on metallic surfaces under ultrahigh vacuum is well-known.[65,66] To the best of our

DOI: 10.1021/ja513263j
J. Am. Chem. Soc. 2015, 137, 2400−2408

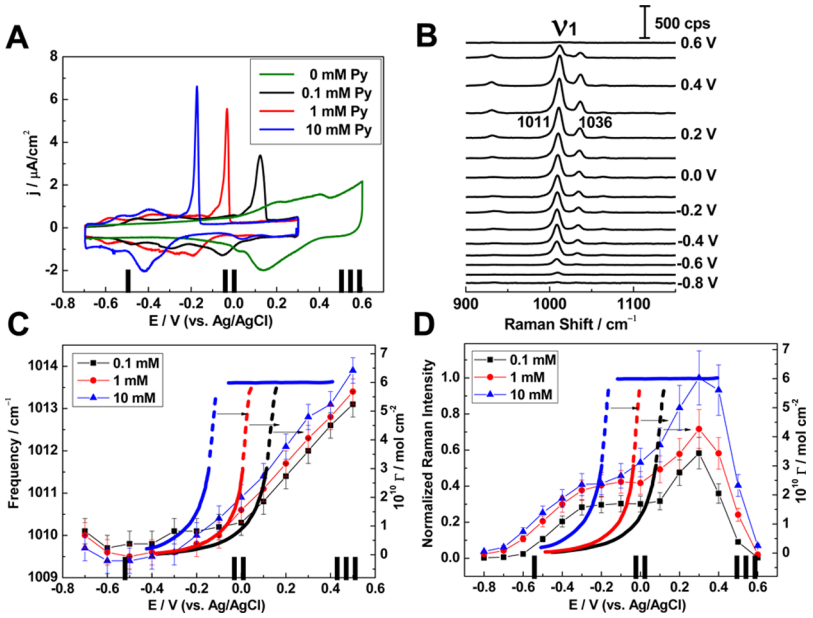

Figure 5. (A) CVs from a Au(100) electrode in 0.1 M $NaClO_4$ solution without pyridine (Py) and with Py at 0.1, 1, and 10 mM. (B) SHINER spectra of Py adsorption on a Au(100) electrode in 0.1 M $NaClO_4$ + 1 mM Py. Acquisition time was 30 s. The dependence of Raman frequency (C) and normalized Raman intensity (D) on applied potential for the Py ν_1 ring breathing mode (data points connected by straight lines), and these are compared to surface concentration isotherms[4] (bold curves).

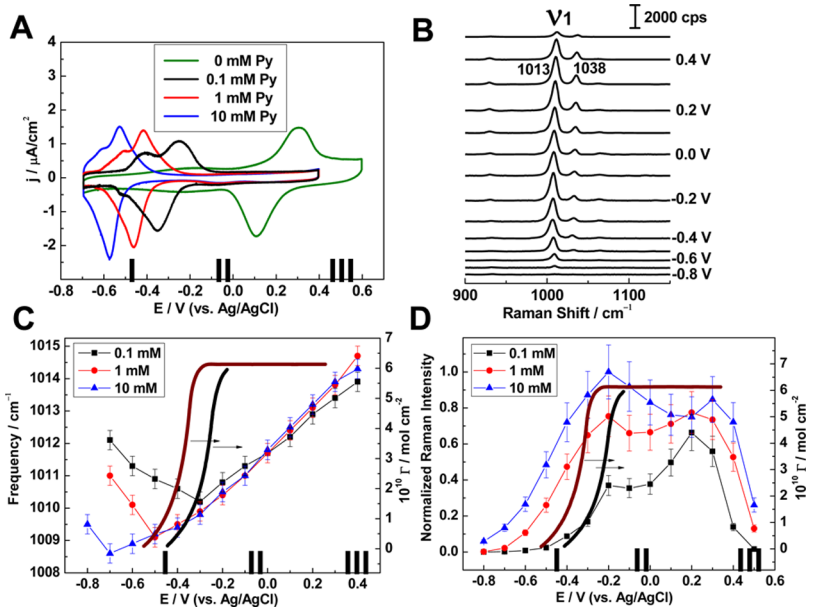

Figure 6. (A) CVs from a Au(110) electrode in 0.1 M $NaClO_4$ solution without pyridine (Py) and with Py at 0.1, 1, and 10 mM. (B) SHINER spectra of Py adsorption on a Au(110) electrode in 0.1 M $NaClO_4$ + 1 mM Py. Acquisition time was 10 s. The dependence of Raman frequency (C) and normalized Raman intensity (D) on applied potential for the Py ν_1 ring breathing mode (data points connected by straight lines), and these are compared to surface concentration isotherms[69] (bold curves). We note that the dark red surface concentration isotherm is for 0.6 mM pyridine.

knowledge, however, this is the first indication of a second pyridine adlayer at an electrified solid/liquid interface.

Pyridine Adsorption on Au(100). Typical CVs from a Au(100) electrode in the absence and presence of pyridine (0.1, 1, and 10 mM) in 0.1 M $NaClO_4$ are provided in Figure 5A. The broad anodic peak obtained at 0.4 V in the absence of pyridine is due to hex-reconstruction lifting.[4,67] In the presence of pyridine in region I, the broad anodic peaks are assigned to adsorption and the broad cathodic peaks are assigned to desorption.[4] The most striking features in the CVs are the sharp peaks in region II at 0.12, −0.03, and −0.18 V for 0.1, 1, and 10 mM pyridine, respectively. These peaks are associated with hex-reconstruction lifting and a π-bonded to N-bonded pyridine phase transition. The unreconstructed Au(100) surface is partially reconstructed when the potential is swept in the negative direction at a slow scan rate.[68] Chronocoulometric and differential capacitance data[4] show that the phase transition in the pyridine adlayer occurs at around 0.08, −0.03, and −0.19 V for 0.1, 1, and 10 mM pyridine, respectively. Our voltammetric data is in good agreement.

DOI: 10.1021/ja513263j
J. Am. Chem. Soc. 2015, 137, 2400−2408

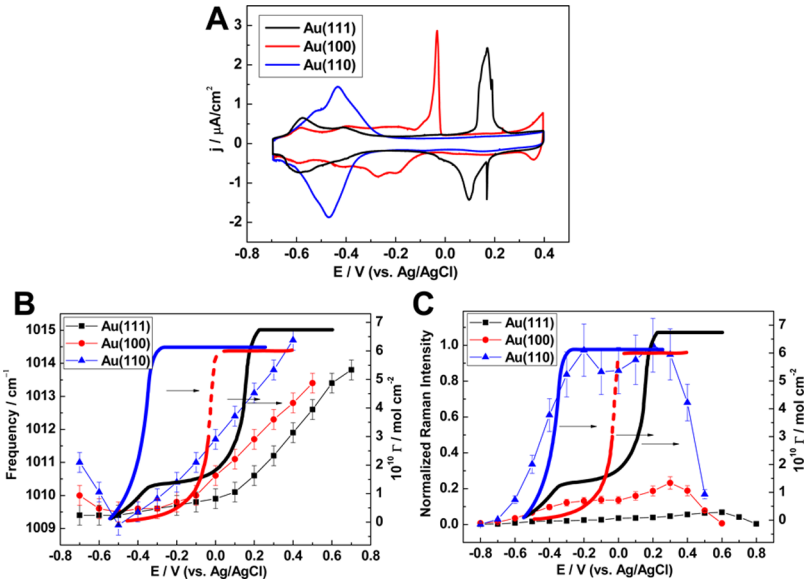

Figure 7. (A) CVs from Au(111), Au(100) and Au(110) electrodes in 0.1 M $NaClO_4$ + 1 mM pyridine. The dependence of Raman frequency (B) and normalized Raman intensity (C) on applied potential for the pyridine 1 ring breathing mode (data points connected by straight lines), and these are compared with surface concentration isotherms (bold curves), on Au(111), Au(100) and Au(110).

Figure 5B shows in situ SHINER spectra of pyridine adsorption on a Au(100) single crystal electrode from 1 mM solution. The ν1 mode frequency (1011 cm^{-1}) is plotted against potential in Figure 5C. Frequency does not change much with potential in region I, but it increases continuously in region II at potentials beyond 0.0, −0.1, and −0.3 V for 0.1, 1, and 10 mM pyridine, respectively. We suggest that the linear increase with a Stark tuning rate of about 5.5 cm^{-1}/V seen for Au(100) is analogous to what was seen for Au(111), and due to increasing bond strength of vertically adsorbed pyridine with the single crystal electrode. Again, frequency increases with increasing pyridine solution concentration at a given potential in region II.

The ν1 peak intensity is plotted against potential in Figure 5D. All three pyridine concentrations show the same trend: the 1011 cm^{-1} peak grows with potential in region I, reaches maximum height at 0.3 V in region II, then drops rapidly to zero at 0.6 V in region III. The dipole−dipole depolarization effect contributes to the maximum at 0.3 V.[27] Surface oxidation, evidenced by the 580 cm^{-1} peak at E ≥ 0.5 V (Supporting Information Figure S5), explains the complete loss of intensity at 0.6 V.

A steep ν1 intensity increase is seen in each of regions I and II (data points connected by straight lines in Figure 5D). The first is due to an increase in the coverage of π-bonded pyridine, as region I is characterized by this process. The onset of the second intensity increase coincides with the position of the pronounced CV peak in region II for respective pyridine concentrations. As we have already explained, hex-reconstruction lifting and a pyridine phase transition occur at this point in the scan. These two processes are followed by an increase in the coverage of N-bonded pyridine (bold curves in Figure 5D).[4] The second intensity increase is therefore due to an increase in the coverage of N-bonded pyridine. Stronger binding of pyridine to Au at more positive surface potentials may also cause the ν1 intensity to increase in region II.

Pyridine Adsorption on Au(110). CVs obtained from a Au(110) electrode in the absence and presence of pyridine (0.1, 1, and 10 mM) in 0.1 M $NaClO_4$ are shown in Figure 6A. The broad peak seen at 0.3 V in the absence of pyridine is probably due to anion adsorption and lifting of the missing-row reconstruction.[69−71] In the presence of pyridine, the anodic and cathodic peaks in region I shift negatively with increasing concentration. The coverage results (bold curves in Figure 6C,D)[69] show that the pyridine monolayer is complete at −0.17 and −0.28 V for 0.1 and 0.6 mM pyridine solution concentrations, respectively. These potentials correspond to the potentials at which the anodic peaks in the 0.1 and 1 mM pyridine CVs return to baseline. Thus, the anodic and cathodic peaks in region I can be assigned to adsorption and desorption of pyridine. On the basis of chronocoulometric and differential capacitance data, it has been proposed that pyridine is vertically adsorbed on Au(110) throughout the −0.7 to 0.6 V potential region,[69] and indeed, our CVs are featureless in region II.

Figure 6B shows in situ SHINER spectra of pyridine adsorption on a Au(110) single crystal electrode from 1 mM solution. No pyridine bands were observed at $E \leq -0.8$ V and $E > 0.5$ V. The ν1 mode frequency is plotted against potential in Figure 6C. Here, ν1 frequency passes through a minimum at −0.3, −0.5, and −0.7 V for 0.1, 1, and 10 mM pyridine. This very interesting result will be discussed shortly. In region II, Au(111) and Au(100) were found to give linearly increasing ν1 frequencies with Stark tuning rates of about 5.6 and 5.5 cm^{-1}/V. Similarly, Au(110) gives a Stark tuning rate of about 5.8 cm^{-1}/V. Such values are characteristic of a vertically adsorbed pyridine monolayer. The frequency increase reflects a stronger binding interaction between pyridine and the Au surface.

The negative ν1 mode Stark tuning rates and the frequency minima seen in Figure 6C have never been reported before. They are unexpected because the ν1 mode frequency usually increases with potential for N-bound pyridine (Figures 3C and 5C). We suggest that increasing pyridine coverage just before the frequency minimum in region I can lead to changes in the pyridine adlayer that favor intermoleculer interactions at the expense of pyridine-Au interactions. A weakening of pyridine-Au interactions would give rise to a negative Stark tuning rate. The effect of increasing pyridine coverage on the Stark tuning rate continues until a full monolayer is formed. For example,

DOI: 10.1021/ja513263j
J. Am. Chem. Soc. 2015, 137, 2400−2408

the pyridine monolayer is complete at −0.3 V in 0.1 mM pyridine (bold black curve), which corresponds to the position of the frequency minimum (data points connected by straight lines). Significantly negative ν1 mode Stark tuning rates were not observed for Au(100) and Au(111) (Figures 3C and 5C) because pyridine adsorbs flat on these faces in region I, whereas it adsorbs vertically on Au(110) in the whole potential window investigated.

For a given potential in region I, ν1 mode frequency is lower at higher pyridine concentrations. This is because pyridine coverage is greater when there is more pyridine in solution, and binding of pyridine to Au(110) is weaker. For a given potential in region II, where for Au(110) the surface is already saturated with N-bound pyridine, all pyridine solution concentrations have similar ν1 mode frequencies.

The ν1 peak intensity is plotted against potential in Figure 6D. It increases in region I as pyridine coverage increases, reaching a maximum at −0.2 V where a full monolayer is formed. A second maximum, which may be due to the charge transfer enhancement mechanism,[24,30,72,73] is seen at about 0.2 V in region II. A transfer of negative charge from Au to pyridine can enhance the ν1 peak intensity if the energy difference is tuned to match the energy of the incident light through the applied potential.[74] Finally, the ν1 peak intensity decreases because of Au surface oxidation. The peak at ∼560 cm^{-1} (Supporting Information Figure S6) is evidence of this oxidation.

Comparison of Three Basal Au(hkl) Faces. Figure 7 provides a comparison of the data obtained for three basal Au(hkl) faces in 1 mM pyridine. CVs from the three faces show the importance of electrode surface structure on pyridine adsorption. Potentials for the completion of a pyridine monolayer decrease in the following order: Au(111) at 0.24 V > Au(100) at −0.04 V > Au(110) at −0.27 V. This trend follows the sequence of E_{pzc} values obtained in the absence of pyridine,[63] and suggests that the electrode charge plays a key role in the adsorption process. Potentials of complete monolayer formation are compared with E_{pzc} values in Table 1.

Table 1. Potentials Comparison of the Pyridine Monolayer Completion and E_{pzc} for Au(hkl) Electrodes[a]

electrode	monolayer completion (V)	E_{pzc} (V)
Au(111)	0.24	0.33
Au(100)	−0.04	0.19
Au(110)	−0.27	0.06

[a]Potentials for the completion of a pyridine monolayer in 0.1 M $KClO_4$ + 1 mM pyridine[4,59,69] and E_{pzc} values obtained in 0.1 M $KClO_4$[48] are compared for Au(hkl) electrodes. All potentials given are versus a Ag/AgCl reference.

The ν1 frequencies for the three Au(hkl) faces show similar trends when plotted against potential, but they increase in magnitude at a given potential when $E \geq -0.1$ V in the following order: Au(111) < Au(100) < Au(110). Again, this order coincides with the trend in E_{pzc} values. It suggests that the binding interaction between pyridine and Au(hkl) is affected by surface charge and becomes stronger after complete formation of a pyridine monolayer in the order Au(111) < Au(100) < Au(110).

The ν1 peak intensity for adsorbed pyridine increases as Au(111) < Au(100) ≪ Au(110). The enhancement factors amount to 8.6×10^4 at 0.6 V for Au(111), 2.6×10^5 at 0.3 V for Au(100) and 1.2×10^6 at 0.2 V for Au(110). This facet-dependence of SHINERS intensity can be explained in terms of the dielectric properties of the single crystal surfaces, which lead to considerably different electromagnetic field coupling strengths for our SHINERS nanoparticles and the different single crystal surfaces.[49]

Analytical Figures of Merit. In the previous sections we have demonstrated that EC-SHINERS is a very powerful technique for the in situ monitoring of adsorption on well-defined single crystal surfaces. We now examine some of the figures of merit for this technique, and compare it to other Raman-based spectroscopic methods.

Selectivity for the Surface of Interest over the Surface of a Plasmonic Substrate. It is desirable to characterize electrochemical processes by SERS because of the high sensitivity and rich structural information that SERS can offer. Traditionally, however, a nanostructured surface of Au, Ag or Cu is required to support the SPRs necessary for SERS. If a plasmonic substrate is introduced into the system because the electrode surface is not of the right morphology or material for SERS, signal from molecules on the substrate will be obtained simultaneously with signal from molecules on the electrode. In EC-SHINERS, the plasmonic substrate is isolated from the chemical system by some inert material so that only signal from the analyte on the electrode is obtained.

Selectivity for Adsorbed Molecules over Molecules in Solution. If the isolating material is chosen correctly and the analyte is not adsorbed, then all of the signal originates from the analyte on the surface of interest. This is because electromagnetic field strength decays exponentially with distance from a plasmonic substrate,[57] and when analytes are in solution, an insufficient number of molecules lie close enough to the surface to generate a detectible signal.

Sensitivity. In some cases, TERS might be used to achieve separation of the plasmonic substrate from the electrochemical system under study. Although the enhancement factor of a tip can be large, the signal obtained from a single tip is much smaller than that obtained from a layer of SHINERS nanoparticles. If each SHINERS nanoparticle acts as a signal enhancing tip, the equivalent of about 1000 tips are excited at the same time when SHINERS nanoparticles having a 55 nm core fill a 2 μm laser spot.

Reliability for the Detection of Molecular/Metal-Molecule Changes. Like SERS, EC-SHINERS is an extremely sensitive, high-resolution fingerprint vibrational spectroscopy. It can access the low wavenumber spectral region and therefore provide direct information about metal-molecule interactions. All of this means that a change in EC-SHINERS signal will be obtained for any molecular/metal-molecule change at the electrode−solution interface.

Reproducibility. SHINERS nanoparticles provide more stable and more reproducible Raman signals than other SERS substrates because the signal amplifier is protected by an inert shell. They give stable Raman frequencies and intensities for days, either in solution or on a solid surface. In addition, SHINERS nanoparticles easily form a uniform submonolayer or full monolayer on a surface, which increases the EC-SHINERS measurement reproducibility.

Minimal Time and Cost Requirements. SHINERS nanoparticles require just a few hours to prepare. Furthermore, the reagents specified in a recently published protocol[56] cost no more than $500 US. This price is an upper limit for the initial investment, as it includes the cost of pyridine (for quality

DOI: 10.1021/ja513263j
J. Am. Chem. Soc. 2015, 137, 2400−2408

assurance testing[44,45,55,56]) as well as the cost of the reagents necessary to prepare aqua regia and piranha solutions (for cleaning of glassware). Once the SHINERS synthesis is operational, the cost is about $0.50 US for 30 mL of nanoparticle solution. Since EC-SHINERS does not require a lot of resources, it is accessible to any organization with a bit of experience in chemical synthesis.

CONCLUSIONS

With SHINERS, it is possible to obtain high-quality Raman spectra from pyridine on Au(111), Au(100) and Au(110) surfaces in an electrochemical environment. Notably, the effects of crystallographic orientation, pyridine concentration, and applied potential on pyridine adsorption were systematically studied using EC-SHINERS. By combining SHINERS results with voltammetric data, as well as chronocoulometric data, we found that increases in the ν1 ring breathing mode frequency and intensity are due to Au surface structure transitions and flat π-bonded/vertical N-bonded pyridine reorientations. Furthermore, EC-SHINERS revealed for the first time the formation of a second pyridine adlayer on Au(111). Electrochemical and SHINERS results correlated very well throughout this work. In essence, we have demonstrated that EC-SHINERS is a powerful spectroscopic method with tremendous potential for the study of structurally well-defined surfaces, such as those used in surface science, electrochemistry and catalysis. We hope this study will increase the depth and breadth of SHINERS applications in a variety of chemical reactions occurring at interfaces.

EXPERIMENTAL SECTION

Chemicals. Chloroauric acid ($HAuCl_4 \cdot 3H_2O$, 99.99%), sodium citrate (99.0%), (3-aminopropyl)trimethoxysilane (97%) and sodium perchlorate (98.0% to 102.0%) were purchased from Alfa Aesar; sodium silicate solution (27% SiO_2) and pyridine (≥99.8%) were purchased from Sigma-Aldrich. All chemicals were used as received without further purification. Argon (99.999%) was purchased from Alphagas. Water was purified with a Milli-Q system (18.2 MΩ cm, 2 ppb total organic carbon).

Preparation of Au(hkl) Single Crystal Electrodes. The electrodes used were Clavilier-type Au(hkl) half-bead single crystals with a diameter of ~2 mm (Figure 2B). Island-free, unreconstructed Au(hkl)-(1 × 1) electrodes were prepared according to the procedure given by Hölzle et al.[75] Briefly, the electrodes were annealed in a butane flame for 2 min and cooled to room temperature in an argon atmosphere. The flame-annealed Au(hkl) electrodes were then immersed in 10 mM hydrochloric acid for 10 min to lift the reconstruction and make island-free Au(hkl)-(1 × 1) surfaces with rather large terraces (Figure 2C) for subsequent modification. Chloride ions were removed by rinsing the electrodes with Milli-Q water and drying them in a stream of argon. The electrodes were brought into contact with the electrolyte solutions at −0.35 V (versus a Ag/AgCl reference electrode), and potential cycling was initiated in the negative direction. Our procedures for preparing Au@SiO_2 SHINERS nanoparticles, modifying Au(hkl) electrodes with these nanoparticles, and cleaning are described in Results and Discussion.

Electrochemical Measurements. Electrochemical measurements were conducted in a three-compartment glass cell containing 0.1 M $NaClO_4$ solution, a Pt coil auxiliary electrode, and a Ag/AgCl reference electrode (all potentials given in this work are relative to a Ag/AgCl reference). Argon was used to deaerate the solutions, and argon was also passed over the solutions during our experiments. The freshly prepared electrodes were brought into contact with the electrolyte in a hanging meniscus configuration under potential control. Electrochemical measurements were carried out with an Autolab PGSTAT30 (Metrohm).

Raman Measurements. Raman spectra were acquired with a LabRam HR800 confocal microprobe Raman system (HORIBA Jobin Yvon). The excitation wavelength was 632.8 nm from a He−Ne laser, and power on the sample was about 1 mW. A 50× magnification long working distance (8 mm) objective was used to focus the incident laser light onto the sample and collect the backscattered light. Raman frequencies were calibrated using Si wafer and $NaClO_4$ solution spectra. Error bars represent standard deviations obtained by making measurements at different locations on the samples. A homemade spectroelectrochemical cell with a Pt wire counter electrode and a Ag/AgCl reference electrode was used for the electrochemical SERS measurements. Pyridine solutions were deaerated with argon and then injected into the spectroelectrochemical cell through Teflon tubing. Electrochemical control was achieved with a home-built potentiostat and software developed in our group.

ASSOCIATED CONTENT

Supporting Information

CVs showing that the HER cleaning procedure is effective. SHINER spectra of pyridine adsorption on Au(111), Au(100) and Au(110) electrodes with expanded spectral range. This material is available free of charge via the Internet at http://pubs.acs.org.

AUTHOR INFORMATION

Corresponding Author

li@xmu.edu.cn

Notes

The authors declare no competing financial interest.

ACKNOWLEDGMENTS

This research was supported by the Thousand Youth Talents Plan of China, the Ministry of Science and Technology (MOST) of China (2011YQ030124), the Swiss National Science Foundation (200020-144471, and 200021-124643), EC FP7 ITN "MOLESCO" project (606728).

REFERENCES

(1) Van Duyne, R. P. In *Chemical and Biochemical Applications of Lasers*; Moore, C. B., Ed.; Academic Press: New York, 1979; Vol. 4, p 101.
(2) Fleischmann, M.; Hill, I. R. In *Comprehensive Treatise of Electrochemistry*; White, R. E., Bockris, J. O. M., Conway, B. E., Yeager, E., Eds.; Plenum Press: New York, 1984; Vol. 8, p 373.
(3) Pettinger, B. In *Adsorption at Electrode Surface*; Lipkowski, J., Ross, P. N., Eds.; VCH: New York, 1992; p 285.
(4) Stolberg, L.; Lipkowski, J.; Irish, D. E. *J. Electroanal. Chem.* **1987**, *238*, 333.
(5) Lipkowski, J.; Stolberg, L.; Morin, S.; Irish, D. E.; Zelenay, P.; Gamboa, M.; Wieckowski, A. *J. Electroanal. Chem.* **1993**, *355*, 147.
(6) Henglein, F.; Lipkowski, J.; Kolb, D. M. *J. Electroanal. Chem.* **1991**, *303*, 245.
(7) Pettinger, B.; Lipkowski, J.; Mirwald, S.; Friedrich, A. *J. Electroanal. Chem.* **1992**, *329*, 289.
(8) Hebert, P.; Le Rille, A.; Zheng, W. Q.; Tadjeddine, A. *J. Electroanal. Chem.* **1998**, *447*, 5.
(9) Andreasen, G.; Vela, M. E.; Salvarezza, R. C.; Arvia, A. J. *Langmuir* **1997**, *13*, 6814.
(10) Cai, W. B.; Wan, L. J.; Noda, H.; Hibino, Y.; Ataka, K.; Osawa, M. *Langmuir* **1998**, *14*, 6992.
(11) Fleischmann, M.; Hendra, P. J.; McQuillan, A. J. *Chem. Phys. Lett.* **1974**, *26*, 163.
(12) Jeanmaire, D. L.; Van Duyne, R. P. *J. Electroanal. Chem.* **1977**, *84*, 1.
(13) Albrecht, M. G.; Creighton, J. A. *J. Am. Chem. Soc.* **1977**, *99*, 5215.

DOI: 10.1021/ja513263j
J. Am. Chem. Soc. 2015, 137, 2400−2408

(14) Nie, S. M.; Emery, S. R. *Science* **1997**, *275*, 1102.
(15) Nie, S. M.; Zare, R. N. *Annu. Rev. Biophys. Biomol. Struct.* **1997**, *26*, 567.
(16) Kneipp, K.; Wang, Y.; Kneipp, H.; Perelman, L. T.; Itzkan, I.; Dasari, R.; Feld, M. S. *Phys. Rev. Lett.* **1997**, *78*, 1667.
(17) Michaels, A. M.; Nirmal, M.; Brus, L. E. *J. Am. Chem. Soc.* **1999**, *121*, 9932.
(18) Xu, H. X.; Bjerneld, E. J.; Kall, M.; Borjesson, L. *Phys. Rev. Lett.* **1999**, *83*, 4357.
(19) McCreery, R. L. *Raman Spectroscopy for Chemical Analysis*; John Wiley: New York, 2000.
(20) *Surface Enhanced Raman Scattering*; Chang, R. K., Furtak, T. E., Eds.; Plenum Press: New York, 1982.
(21) *Surface Enhanced Raman Vibrational Studies at Solid/Gas Interfaces, Springer Tracts in Modern Physics*; Pockrand, I., Ed.; Springer: New York, 1984; Vol. *104*.
(22) Moskovits, M. *Rev. Mod. Phys.* **1985**, *57*, 783.
(23) Birke, R. L.; Lu, T.; Lombardi, J. R. In *Techniques for Characterization of Electrodes and Electrochemical Processes*; Varma, R., Selman, J. R., Eds.; John Wiley & Sons: New York, 1991.
(24) Wu, D. Y.; Li, J. F.; Ren, B.; Tian, Z. Q. *Chem. Soc. Rev.* **2008**, *37*, 1025.
(25) Camden, J. P.; Dieringer, J. A.; Zhao, J.; Van Duyne, R. P. *Acc. Chem. Res.* **2008**, *41*, 1653.
(26) Zheng, J.; Jiao, A. L.; Yang, R. H.; Li, H. M.; Li, J. S.; Shi, M. L.; Ma, C.; Jiang, Y.; Deng, L.; Tan, W. H. *J. Am. Chem. Soc.* **2012**, *134*, 19957.
(27) Stolberg, L.; Lipkowski, J.; Irish, D. E. *J. Electroanal. Chem.* **1991**, *300*, 563.
(28) Tian, Z. Q.; Ren, B.; Wu, D. Y. *J. Phys. Chem. B* **2002**, *106*, 9463.
(29) Wu, D. Y.; Ren, B.; Jiang, Y. X.; Xu, X.; Tian, Z. Q. *J. Phys. Chem. A* **2002**, *106*, 9042.
(30) Zhao, L. L.; Jensen, L.; Schatz, G. C. *J. Am. Chem. Soc.* **2006**, *128*, 2911.
(31) Stolberg, L.; Lipkowski, J.; Irish, D. E. *J. Electroanal. Chem.* **1991**, *300*, 563.
(32) Tian, Z. Q.; Ren, B.; Li, J. F.; Yang, Z. L. *Chem. Commun.* **2007**, 3514.
(33) Nikoobakht, B.; El-Sayed, M. A. *Chem. Mater.* **2003**, *15*, 1957.
(34) Guerrini, L.; McKenzie, F.; Wark, A. W.; Faulds, K.; Graham, D. *Chem. Sci.* **2012**, *3*, 2262.
(35) Moskovits, M. *J. Raman Spectrosc.* **2005**, *36*, 485.
(36) Willets, K. A.; Van Duyne, R. P. *Annu. Rev. Phys. Chem.* **2007**, *58*, 267.
(37) Le, F.; Lwin, N. Z.; Halas, N. J.; Nordlander, P. *Phys. Rev. B: Condens. Matter Mater. Phys.* **2007**, *76*, 165410.
(38) Tian, Z. Q.; Ren, B. *Annu. Rev. Phys. Chem.* **2004**, *55*, 197.
(39) Campion, A.; Mullins, D. R. *Chem. Phys. Lett.* **1983**, *94*, 576.
(40) Bruckbauer, A.; Otto, A. *J. Raman Spectrosc.* **1998**, *29*, 665.
(41) Stockle, R. M.; Suh, Y. D.; Deckert, V.; Zenobi, R. *Chem. Phys. Lett.* **2000**, *318*, 131.
(42) Pettinger, B.; Ren, B.; Picardi, G.; Schuster, R.; Ertl, G. *Phys. Rev. Lett.* **2004**, *92*, 096101.
(43) Ren, B.; Picardi, G.; Pettinger, B.; Schuster, R.; Ertl, G. *Angew. Chem., Int. Ed.* **2005**, *44*, 139.
(44) Li, J. F.; Huang, Y. F.; Ding, Y.; Yang, Z. L.; Li, S. B.; Zhou, X. S.; Fan, F. R.; Zhang, W.; Zhou, Z. Y.; Wu, D. Y.; Ren, B.; Wang, Z. L.; Tian, Z. Q. *Nature* **2010**, *464*, 392.
(45) Anema, J. R.; Li, J. F.; Yang, Z. L.; Ren, B.; Tian, Z. Q. *Annu. Rev. Anal. Chem.* **2011**, *4*, 129.
(46) Graham, D. *Angew. Chem., Int. Ed.* **2010**, *49*, 9325.
(47) Liu, B.; Blaszczyk, A.; Mayor, M.; Wandlowski, T. *ACS Nano* **2011**, *5*, 5662.
(48) Honesty, N. R.; Gewirth, A. A. *J. Raman Spectrosc.* **2012**, *43*, 46.
(49) Li, J. F.; Ding, S. Y.; Yang, Z. L.; Bai, M. L.; Anema, J. R.; Wang, X.; Wang, A.; Wu, D. Y.; Ren, B.; Hou, S. M.; Wandlowski, T.; Tian, Z. Q. *J. Am. Chem. Soc.* **2011**, *133*, 15922.
(50) Li, J. F.; Anema, J. R.; Yu, Y. C.; Yang, Z. L.; Huang, Y. F.; Zhou, X. S.; Ren, B.; Tian, Z. Q. *Chem. Commun.* **2011**, *47*, 2023.
(51) Butcher, D. P.; Boulos, S. P.; Murphy, C. J.; Ambrosio, R. C.; Gewirth, A. A. *J. Phys. Chem. C* **2012**, *116*, 5128.
(52) Lin, L.; Tian, X. D.; Hong, S. L.; Dai, P.; You, Q. C.; Wang, R. Y.; Feng, L. S.; Xie, C.; Tian, Z. Q.; Chen, X. *Angew. Chem., Int. Ed.* **2013**, *52*, 7266.
(53) Tittl, A.; Yin, X. H.; Giessen, H.; Tian, X. D.; Tian, Z. Q.; Kremers, C.; Chigrin, D. N.; Liu, N. *Nano Lett.* **2013**, *13*, 1816.
(54) Frens, G. *Nat., Phys. Sci.* **1973**, *241*, 20.
(55) Li, J. F.; Li, S. B.; Anema, J. R.; Yang, Z. L.; Huang, Y. F.; Ding, Y.; Wu, Y. F.; Zhou, X. S.; Wu, D. Y.; Ren, B.; Wang, Z. L.; Tian, Z. Q. *Appl. Spectrosc.* **2011**, *65*, 620.
(56) Li, J. F.; Tian, X. D.; Li, S. B.; Anema, J. R.; Yang, Z. L.; Ding, Y.; Wu, Y. F.; Zeng, Y. M.; Chen, Q. Z.; Ren, B.; Wang, Z. L.; Tian, Z. Q. *Nat. Protoc.* **2013**, *8*, 52.
(57) Zayats, A. V.; Smolyaninov, I. I.; Maradudin, A. A. *Phys. Rep.* **2005**, *408*, 131.
(58) Li, J. F.; Rudnev, A.; Fu, Y. C.; Bodappa, N.; Wandlowski, T. *ACS Nano* **2013**, *7*, 8940.
(59) Stolberg, L.; Morin, S.; Lipkowski, J.; Irish, D. E. *J. Electroanal. Chem.* **1991**, *307*, 241.
(60) Creighton, J. A.; Blatchford, C. G.; Albrecht, M. G. *J. Chem. Soc., Faraday Trans. 2* **1979**, *75*, 790.
(61) Moskovits, M.; Dilella, D. P. *J. Chem. Phys.* **1980**, *73*, 6068.
(62) Zhang, Y.; Gao, X. P.; Weaver, M. J. *J. Phys. Chem.* **1993**, *97*, 8656.
(63) Lipkowski, J.; Stolberg, L.; Yang, D. F.; Pettinger, B.; Mirwald, S.; Henglein, F.; Kolb, D. M. *Electrochim. Acta* **1994**, *39*, 1045.
(64) Li, N. H.; Zamlynny, V.; Lipkowski, J.; Henglein, F.; Pettinger, B. *J. Electroanal. Chem.* **2002**, *524*, 43.
(65) Zhong, Q.; Gahl, C.; Wolf, M. *Surf. Sci.* **2002**, *496*, 21.
(66) Bahr, S.; Kempter, V. *J. Chem. Phys.* **2007**, 127.
(67) Kolb, D. M. *Prog. Surf. Sci.* **1996**, *51*, 109.
(68) Skoluda, P.; Holzle, M.; Lipkowski, J.; Kolb, D. M. *J. Electroanal. Chem.* **1993**, *358*, 343.
(69) Stolberg, L.; Lipkowski, J.; Irish, D. E. *J. Electroanal. Chem.* **1990**, *296*, 171.
(70) Magnussen, O. M.; Wiechers, J.; Behm, R. J. *Surf. Sci.* **1993**, *289*, 139.
(71) Kolb, D. M. *Prog. Surf. Sci.* **1996**, *51*, 109.
(72) Wu, D. Y.; Hayashi, M.; Lin, S. H.; Tian, Z. Q. *Spectrochim. Acta, Part A* **2004**, *60*, 137.
(73) Otto, A.; Mrozek, I.; Grabhorn, H.; Akemann, W. *J. Phys.: Condens. Matter* **1992**, *4*, 1143.
(74) Wu, D. Y.; Liu, X. M.; Duan, S.; Xu, X.; Ren, B.; Lin, S. H.; Tian, Z. Q. *J. Phys. Chem. C* **2008**, *112*, 4195.
(75) Holzle, M. H.; Wandlowski, T.; Kolb, D. M. *J. Electroanal. Chem.* **1995**, *394*, 271.

DOI: 10.1021/ja513263j
J. Am. Chem. Soc. 2015, 137, 2400−2408